LAWRENCE
LIVERMORE
NATIONAL
LABORATORY

LLNL-TR-659685

Standard Diagnostics for the Diurnal Cycle of Precipitation

C. Covey, P. Gleckler

September 3, 2014

Disclaimer

This work performed under the auspices of the U.S. Department of Energy by Lawrence Livermore National Laboratory under Contract DE-AC52-07NA27344.

Standard Diagnostics for the Diurnal Cycle of Precipitation

Curt Covey and Peter Gleckler
Program for Climate Model Diagnosis and Intercomparison
Lawrence Livermore National Laboratory
<covey1@llnl.gov>
September 2014

Introduction

The purpose of this document is to suggest a strategy for constructing standard diagnostics of the diurnal cycle from both climate model and observational data products. The guiding philosophy is "keep it simple," in the hope that a diagnostic software package can be readily constructed and widely used. Of course this means that the output of the package will form only the beginning of necessary examination of the diurnal cycle in models and in the real world.

The latest version of the Coupled Model Intercomparison Project, CMIP5, provides several fields at 3-hourly time resolution near the surface: air and surface temperatures, pressure, humidity, soil moisture, horizontal wind, energy flux components, overhead cloudiness, evaporation, precipitation, convective precipitation, and snowfall. (See the "3hr" tab in the Standard Output spreadsheet at http://cmip-pcmdi.llnl.gov/cmip5/data_description.html.) Meanwhile satellite observations provide at least equally fine time resolution and global coverage for some of these fields. This data makes possible an extensive study of the diurnal cycle near the surface.

Covey et al. (2011, 2014) have published analyses of CMIP 3-hourly surface pressure fields and shown them to be consistent with the conventional picture of "atmospheric tides." Like their oceanic relatives, atmospheric tides are periodic in time and spatially simple at large scales. Thus the surface-pressure tides provide an easy starting point for study of the diurnal cycle. At the opposite end of the complexity scale, precipitation is very irregular in space and time. This document will use precipitation as an example of the challenges to construction of standard diagnostics of the diurnal cycle.

Analysis of the diurnal cycle of a time series $x(t)$ typically begins by forming a "composite" or average diurnal cycle spanning $0 < t < 24$ hours. Then further processing such as Fourier analysis is applied to the composite. Two questions arise: (1) What further processing is most appropriate for simple standard diagnostics that can produce a few key "metric" numbers when climate models are compared with each other or with observations? (2) Is it necessary to form a composite in the first place? Below we argue that (1) straighforward Fourier analysis is the most appropriate procedure and (2) forming a diurnal cycle composite is not necessary because Fourier analysis of $x(t)$ over its entire domain gives the same once-a-day (24h), twice-a-day (12h) and higher harmonics of the diurnal cycle.

A note on definitions: In the study of tides the once-a-day Fourier harmonic is traditionally called "diurnal," the twice-a-day harmonic "semidiurnal," the thrice-a-day harmonic "terdiurnal," and so on. Since the term "diurnal" also refers to the full cycle of a function over the span of one day, before decomposition into Fourier harmonics, we avoid the traditional terms and simply refer to 24- 12-, 8-, ... hour harmonics. Note that our harmonics are fractions of a *solar* day, exactly 24 hours. Gravitationally driven

tides occur at fractions of a *siderial* day, the period of Earth's rotation (0.997 solar days) but the phenomena discussed here (including atmospheric tides) are primarily driven by solar forcing.

(1) Methods of Analysis

Dai et al. (2007) made a composite diurnal cycle of precipitation at each latitude / longitude grid point for December-January-February and June-July-August over several years. Then they least-squares fit 24- and 12-hour cycles to each grid point's composite. The adjustable parameters in each fit are the amplitude and phase of the cycle. Finally they mapped the amplitude (as a percentage of daily mean precip) and the phase (as time of maximum) for both the 24- and 12-hour fits at both seasons: 8 maps in all. At this point the results can be used to produce standard metrics. An important caveat is that for time-of-maximum comparisons, one must use modular arithmetic: 24h = 0h for the once-a-day harmonic, 12h = 0h for the twice-a-day harmonic, and so on.

This procedure is commonly used for diurnal cycle analysis, but there are others. Kikuchi and Wang (2008) simply mapped the climatological mean of the difference between daily-maximum and daily-minimum precipitation as a measure of diurnal cycle amplitude. For DJF and JJA seasons and for the annual mean, this produces 3 maps. To examine the phase, they computed Empirical Orthogonal Eigenfunctions from a composite diurnal cycle. With data from the Tropical Rainfall Measurement MIssion (TRMM) satellite, they found that the first two EOFs represented the 24-hour harmonic and the next two represented the 12-hour harmonic. They plotted time series of the corresponding EOF amplitudes (principal components) for DJF and JJA seasons. For each season and harmonic component, this procedure summarizes both amplitude and phase in only 2 line plots of precipitation rate spanning $0 < t < 24$ hours (as opposed to the initial composites in this procedure and Dai et al.'s, which amount to a line plot for each grid point). Here again the results can be used to produce standard metrics. Wang et al. (2011) propose diagnostic metrics based entirely on such EOFs.

By construction, EOFs provide the most compact representation of the principal variations of space-time fields. They have been popular diagnostics since their introduction to meteorology and climatology by Lorenz (1956) and Kutzbach (1967). Compared with Fourier analysis, however, EOFs are not as simple conceptually and not as accessible computationally. Although the basic principle is simple -- find the eigenvectors and eigenvalues of a correlation matrix -- in practice EOFs come in a variety of versions, each with its own set of advantages and disadvantages (see e.g. Trenberth et al. 2005). Thus they seem inconsistent with a "keep it simple" philosophy for standard diagnostics.

(2) Are Composites Necessary?

To analyze 3-hourly surface pressure output from climate models, Covey et al. (2011, 2014) did not form a diurnal cycle composite. They simply applied a Fast Fourier Transform at each grid point to a 32-day detrended time series of anomalies, i.e. values obtained during each day by subtracting that day's mean value. The Fourier analysis produces harmonic components with periods of 32 days, 16 days and so on, but only the 24h and 12h harmonics were studied. Procedural details probably make little difference to studying pheonomena as regular as the tides. Indeed, Covey et al. showed that their model analysis agrees well with observational analysis of the tides by Dai and Wang (1999) using the compos-

ite technique. But one might worry that the details make a great deal of difference for the diurnal cycle of precipitation.

At first sight a straight-out Fourier analysis seems rather different from the procedure of Dai et al. described above. The differences, however, are more apparent than real. Although Dai et al. used a least-squares fit of the 24- and 12-hour cycles to their composite, it is well known that when a periodic function is approximated by a trigonometric series via least squares, the resulting coefficients are identical to those obtained by Fourier analysis (e.g. Elmore and Heald 1969, Problem 1.7.2). So the question "Are the two procedures equivalent?" becomes "Does it matter whether or not a composite is formed before doing the Fourier analysis?" In fact it does not matter, because time-averaging (which forms the composite) and Fourier-transforming are basically linear integral operations that commute. This is shown below, first assuming for simplicity that time is a continuous variable, then for the more pertinent case in which time is measured in discrete steps.

Continuous Time

Taking the units of local solar time t in days, and considering the time period $0 < t < N$ days, the Fourier series for a function over this domain is

$$x(t) = \sum_{m=-\infty}^{\infty} a_m \, e^{2\pi i m t/N} \; ; \qquad a_m = a_{-m}^{*} \text{ for real } x. \tag{1}$$

Note that Eq. (1) always forces $x(N) = x(0)$ so that outside the domain $0 < t < N$, $x(t)$ repeats with time period N. Thus a trend in x over its nominal domain implies a repeating saw-tooth pattern that can be problematic in Fourier analysis. For this reason it is customary to first de-trend the data.

From the orthogonality of trigonometric functions it follows that

$$a_m = N^{-1} \int_0^N x(t) \, e^{-2\pi i m t/N} \, dt. \tag{2}$$

As with any continuous-time Fourier series, a_0 gives the (constant) average of x over the domain, the $a_{\pm 1}$ give amplitude and phase for the longest allowed period (N days), the $a_{\pm 2}$ give amplitude and phase for half this period ($N/2$ days), the $a_{\pm 3}$ give amplitude and phase for a third this period ($N/3$ days), and so on ad infinitum. But for the diurnal cycle, the only relevant coefficients are $a_{\pm N}$ for the 24-hour harmonic, $a_{\pm 2N}$ for the 12-hour harmonic, $a_{\pm 3N}$ for the 8-hour harmonic, and so on. For comparison with the composite diurnal cycle, it is convenient to write these coefficients as

$$a_{nN} = N^{-1} \int_0^N x(t) \, e^{-2\pi i n t} \, dt = N^{-1} \sum_{k=1}^{N} \int_{k-1}^{k} x(t) \, e^{-2\pi i n t} \, dt. \tag{3}$$

The composite itself is formed by averaging over the time of each day:

$$\bar{x}(t) = N^{-1} \sum_{k=1}^{N} x(t + k - 1) \; ; \qquad 0 < t < 1, \tag{4}$$

e.g. the composite 0800h LST value is $\bar{x}\left(\frac{1}{3}\right) = \left[x\left(\frac{1}{3}\right) + x\left(1 + \frac{1}{3}\right) + x\left(2 + \frac{1}{3}\right) + \ldots + x\left(N - \frac{2}{3}\right)\right] \Big/ N$ in our units.

A Fourier series for $\bar{x}(t)$ is just a special case of Eqs. (1)–(2) with $N = 1$:

$$\bar{x}(t) = \sum_{m=-\infty}^{\infty} \bar{a}_m \, e^{2\pi i m t} \; ; \qquad \bar{a}_m = \bar{a}_{-m}^{*} \text{ for real } \bar{x} \; ; \tag{5}$$

$$\bar{a}_m = \int_0^1 \bar{x}(t) \, e^{-2\pi i m t} \, dt = N^{-1} \int_0^1 \sum_{k=1}^{N} x(t + k - 1) \, e^{-2\pi i m t} \, dt. \tag{6}$$

In this case all of the coefficients that emerge from the procedure are relevant to the diurnal cycle. The $\bar{a}_{\pm 1}$ give amplitude and phase of the 24-hour harmonic, the $\bar{a}_{\pm 2}$ give amplitude and phase of the 12-hour harmonic, the $\bar{a}_{\pm 3}$ give amplitude and phase of the 8-hour harmonic, and so on ad infinitum.

The relationship between the coefficients in Eqs. (3) and (6) is revealed by interchanging the order of summation and integration in (6) and then substituting $t' \equiv t + k - 1$ in the integral. Since the limits $t = 0$

and $t = 1$ become $t' = k - 1$ and $t' = k$, we have

$$\bar{a}_m = N^{-1} \sum_{k=1}^{N} \int_{k-1}^{k} x(t')\, e^{-2\pi i m (t'-k+1)}\, dt'. \qquad (7)$$

After substituting $m \to n$, dropping the prime on the dummy integration variable t', and recognizing that $e^{-2\pi i n (t-k+1)} = e^{-2\pi i n t}$, comparison with Eq. (3) shows that $\bar{a}_n = a_{nN}$ (QED).

A related issue involves Fourier harmonics of spatial averages versus spatial averages of Fourier harmonics. The order of operations should not matter because $\int_t e^{i\omega t} \left[\int_{\text{area}} f(\vec{x}, t)\, d^2x\right] dt = \int_{\text{area}} \left[\int_t e^{i\omega t} f(\vec{x}, t)\, dt\right] d^2x$ as long as the area of integration does not depend on time. In the examples below, we choose to do the Fourier analysis first in order to display maps of amplitude and phase, but the evident (and expected) difference between land and ocean shows that averaging separately over these two areas would be informative.

Discrete Time

Continuing to measure time in days, suppose each day is divided into S time-segments (e.g. $S = 8$ for 3-hourly data) and the continuous function $x(t)$ is replaced by the sequence $x_0, x_1, x_2, \ldots, x_{SN}$ at the segment boundaries over $0 < t < N$. Since x repeats with time period N (q.v.) $x_{SN} = x_0$, so there are exactly $S \times N$ independent time points $x_0, x_1, x_2, \ldots, x_{SN-1}$. The correspondence between $x(t)$ and the x_j is given by $x(t) = x(j/S) \equiv x_j$. Therefore integrals in the equations above are replaced by sums according to

$$\int_a^b f(t)\, dt \to S^{-1} \sum_{j=Sa}^{Sb} f(j/S). \qquad (8)$$

Also, because the interval between time points Δt ($=S^{-1}$days) is finite, a Nyquist limit applies to the highest frequency that can be resolved by Fourier analysis. The equation analogous to (1) is thus

$$x_j = \sum_{m=-SN/2}^{+SN/2} a_m\, e^{2\pi i m j/SN}; \qquad j = 0, 1, 2, \ldots, SN - 1. \qquad (1')$$

At the Nyquist frequency limits $m = \pm SN/2$ the period is twice the interval between time points ($2\,\Delta t = 6$ hours for 3-hourly data). "$2\,\Delta t$ waves" are the highest frequency that discrete Fourier analysis can resolve.

Eq. (1′) represents exactly SN equations in the SN unknowns $a_0, a_{\pm 1}, a_{\pm 2}, \ldots, a_{|SN/2|}$. (The coefficients $a_{-SN/2}$ and $a_{+SN/2}$ represent a single Fourier term because $m = \pm SN/2$ gives the same exponential factor $e^{\pm i\pi j} = (-1)^j$.) These equations can be solved to give

$$a_m = (SN)^{-1} \sum_{j=0}^{SN-1} x_j\, e^{-2\pi i m j/SN} \qquad (2')$$

by using the identity $\sum_{j=0}^{M-1} e^{2\pi i n j/M} = M\,\delta_{nM}$, the discrete version of orthogonality for trigonometric functions (or one may simply apply the transformation (8) to Eq. (2)).

Continuing with this procedure, the analysis of Eqs. (1)–(7) can be repeated to reach the same conclusion. Instead of interchanging the order of summation and integration in going from Eq. (6) to Eq. (7), one interchanges the order of summation in a double sum. In both cases the operations commute, and the 24-hour and higher harmonics are identical whether or not one first forms a composite diurnal cycle.

Caveats

One consideration in deciding between Fourier analysis of a composite diurnal cycle and straight-out Fourier analysis of the original time series is that composites may be useful by themselves. They can be

inspected at a few sample grid points before succeeding steps are taken (e.g. Figure 4 in Dai et al. 2007). None of the above procedures, however, address the “frequency versus intensity” issue of the diurnal cycle of precipitation. For example, the upper left panel of Figure 4 in Dai et al. shows a composite diurnal cycle for the Southeastern USA. This time series has a smooth once-a-day maximum at a well defined time. But the series is an average over many different days. Does the steady increase and then decrease of precipitation rate exhibited by the composite arise from corresponding steady increases and decreases during most days? Or does it arise from different days’ precipitation coming at different times (or not at all) but always at the same rate? Dai et al. argue that the latter explanation is closer to the truth. To make their case, they must reprocess the high-time-frequency raw data in ways that avoid a composite diurnal cycle.

Also, sampling a time series by a moving average inevitably reduces the amplitudes of its Fourier harmonics. This issue is pertinent to the CMIP5 database, in which precipitation and other flux variables are recorded as time averages over successive 3-hour intervals, whereas TRMM observations are snapshots. Dai et al. (1999) point out that time-averaging multiplies a Fourier amplitude at frequency ω by the factor $2\sin(\omega\,\Delta t/2)/\omega\,\Delta t$ (which is always < 1 because $\sin(x)/x < 1$ for all x). In the case of 3-hour averaging intervals $\omega\,\Delta t = \pi/4$, $\pi/2$ and $3\pi/4$ -- and the necessary corrections are about 3%, 10% and 30% -- for the 24-, 12- and 8-hour harmonics respectively. Thus the correction is severe only for the 8-hour harmonic, which is so close to the Nyquist frequency (q.v.) that it should not be taken seriously anyway in 3-hourly data.

Finally, the equivalence between composite and straight-out analysis demonstrated above for the discrete case depends on the time points being evenly spaced. If they are not, then straight-out analysis would naturally give a time point with few or no neighbors on a particular day more weight than a time point on another day with many nearby neighbors. This distinction would be lost on formation of a composite diurnal cycle. For CMIP and Obs4MIPs data, however, the time points are equally spaced, so this caveat does not apply.

(3) Practical Implementation

The equations above are perfectly valid but do not represent the best algorithm for Fourier analysis. The Fast Fourier Transform speeds up the procedure by several orders of magnitude (Press et al. 2007). Standard software packages employ FFTs ubiquitously. For example, Covey et al. wrote scripts in a Python-based climate data analysis language (Williams et al. 2013) that in turn invokes the Numerical Python module **`fft`** for discrete Fourier transforms (http://www.numpy.org). This module is consistent with Eqs. ($1'$) and ($2'$) above, or equivalently Eqs. (12.1.7) and (12.1.9) in Press et al. 2007. Using this software, we produced the two figures shown below from (1) observational data and (2) CMIP5 climate model output, respectively. We obtained observations from the Obs4MIPs project that provides satellite data matched to CMIP output (Teixeira et al. 2014). For 3-hourly precipitation, Obs4MIPs uses TRMM 3B42-3, a standard high-resolution combination of TRMM satellite data with other observations including in situ measurements. For a sample of climate simulation output, we chose GFDL-HIRAM-360 because it has the highest resolution of CMIP5 models providing 3-hourly output, thus potentially the best agreement with observations. TRMM 3B42-3 data covers the globe between about 50°S and 50°N latitudes (rather impressive for a “tropical” dataset!) and we restricted our model output to the same range.

Each figure shows (in the upper panel) precipitation observed during the single month of July 2001 and (in the lower four panels) the corresponding observed amplitudes and phases of the 24- and 12-hour Fourier harmonics. The amplitudes are expressed as a fraction of the monthly mean, so for example an amplitude of 0.3 means that a harmonic component has maximum-to-minimum difference of 60% of the monthly mean. We omitted areas with less than 1.5 mm / day monthly mean precipitation (approximately half the global average) from the amplitude and phase maps, since they seem to give little coherent information about the diurnal cycle; these masked-out areas appear in gray. White colors indicate off-scale high amplitudes.

Perhaps because our figures represent only one month of one year, they are more noisy in appearance than those of other analyses that average over much longer periods of time. For example Dai et al. (2007) and Kikuchi and Wang (2008) average over June-July-August for 8 and 9 years, respectively. Nevertheless our sample results for the TRMM observations are consistent with many features of earlier analyses (e.g. Dai et al., Figs. 5d, 5j, 7c, 7h) including: (1) amplitudes generally larger over land than over ocean; (2) morning maxima over oceans; and (3) late afternoon maxima in the summer monsoon regions of Africa and South/Southeast Asia; and (3) predominance of the 24-hour harmonic, although the 12-hour harmonic is substantial and (generally speaking) tends to reinforce and narrow the precipitation-maximum peak (see Appendix). Also appearing in the TRMM observations of 24-hour component phase, in the center of North America, is a variation of the times of maxima from west to east. The phase variation implies that precipitation begins in the late afternoon over the Rocky Mountains and then moves eastward over the Great Plains from night to morning. This result agrees with reanalysis of high-resolution weather data implying “that the eastward propagation of convection systems from the Rockies to the Great Plains plays an essential role for the warm season climate over the central U.S.” (Jiang et al. 2006).

Also in the TRMM observations of 24-hour component phase, in the Southern midlatitudes, a periodic phase variation appears as stripes running northwest-to-southeast in the Atlantic / Indian Oceans and southwest-to-northeast in the Pacific Ocean. The stripes also appear in the month of January 2002, oriented southwest-to-northeast in both the Atlantic and Pacific Ocean midlatitudes (*not shown here*). Since none of the stripes are oriented precisely north-south, it seems they are not artifacts of the time being recorded at discrete 3-hourly intervals. The stripes may represent the traces of a few individual winter storms over ocean. If so, they should “average out” as we consider longer periods of time -- while simultaneously the central North American phase propagation discussed above becomes more prominent. Although the months of July 2001 and January 2002 are ENSO-neutral in terms of both traditional (Nino3.4) and multi-variable (http://www.esrl.noaa.gov/psd/enso/mei/table.html) indices, and thus may be considered “typical” to a first approximation, detailed analysis of both model simulations and observations requires much more data.

Nevertheless we may comment briefly on the differences shown below between the model output and observations. The model’s monthly mean precipitation looks very similar to the observed field. The model’s Fourier harmonic amplitudes generally agree with observations over land but are too small over tropical oceans, perhaps because sea surface temperature in AMIP-type simulations is prescribed with no diurnal cycle (Gates et al. 1998). An analogous underestimate of surface pressure variations has been noted in model simulations (Covey et al. 2011, 2014). On the other hand, diurnal SST variations are small, so the model may be underestimating the effect upon precipitation of insolation variations between day and night over open-ocean areas (away from land / sea breezes).

The phase maps suggest that the model often produces rainfall too early in the day. Although this discrepancy is a commonly noted problem with weather and climate simulations (e.g. Dai and Trenberth 2004) some of it may be due to observational errors. Kikuchi and Wang (2008) note that the TRMM 3B42-3 dataset includes infrared observations from geosynchronous satellites, and “IR-based precipita-

tion estimates tend to delay by about 3-4 h compared with those measured by ground-based radar or in situ rain gauge data . . . probably because of the contamination of nonprecipitating cirrus anvil clouds which develop after the development of deep convective clouds." On the other hand a different version of the TRMM data, 3G68, "is based only on the TRMM instruments [a microwave imager and precipitation radar], which are believed to provide the most reliable precipitation estimate for the tropics from space." Kikuchi and Wang find that TRMM 3G68 precipitation leads 3B42 by about 3 hours and say "We will therefore adjust the PC [principal component] time series by three hours (according to the PCs in 3G68) when we interpret results of the 3B42 in the discussion throughout the rest of this paper." Making this adjustment would bring the model results shown below into better agreement with observations.

Until we gather more data, we will forego quantification of the differences between various model-produced and observational datasets, such as root-mean-square differences and related statistics (Taylor 2001). Here we only make one comment about the overall amplitudes shown in the figures below. Parseval's Theorem equates the mean-squared value of a time series with a corresponding integral over frequency of its squared Fourier amplitude. Therefore we consider the *square* of the ratio of global mean 24- and 12-hour harmonics in the figures. For the observations this squared ratio is 1.8; for the model it is 2.4. Thus both observations and model have the once-a-day harmonic dominating the twice-a-day harmonic, as asserted above, but the extent of domination seems greater in the model.

Acknowledgments

We thank Aiguo Dai, John Fasullo, Kevin Trenberth and Karl Taylor for useful comments. This work was performed under auspices of the Office of Science, US Department of Energy by Lawrence Livermore National Laboratory under Contract DE-AC52-07NA27344.

Figures

In[4]:=
```
Import["/Users/covey1/CMIP5/Tides/OtherFields/3hrStdDiagnostics/figure1_minus
    _colorwheels.pdf"]
```

Out[4]=

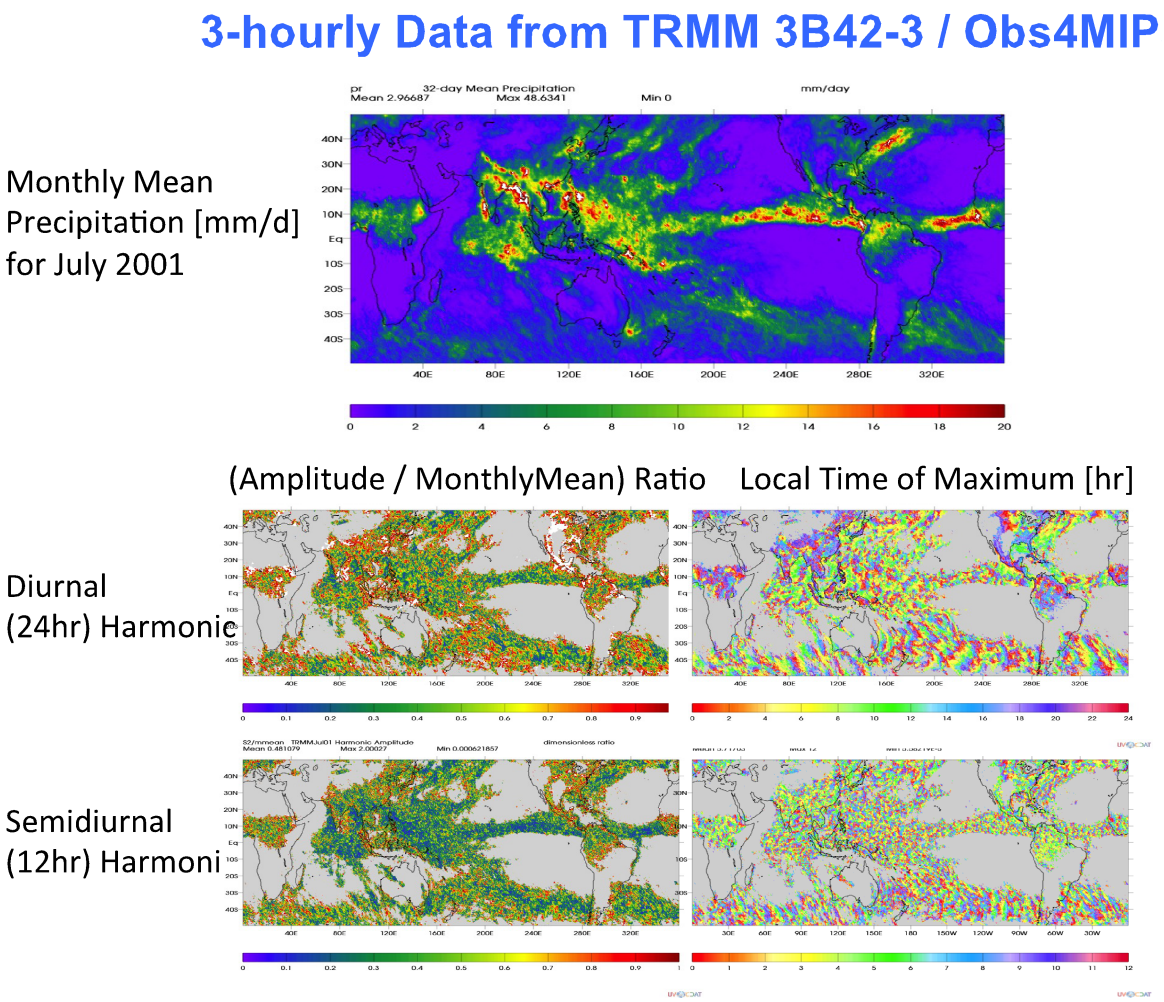

In[5]:=
```
Import["/Users/covey1/CMIP5/Tides/OtherFields/3hrStdDiagnostics/figure2_minus
    _colorwheels.pdf"]
```

Out[5]=

3-hourly Data from GFDL-HIRAM-C360

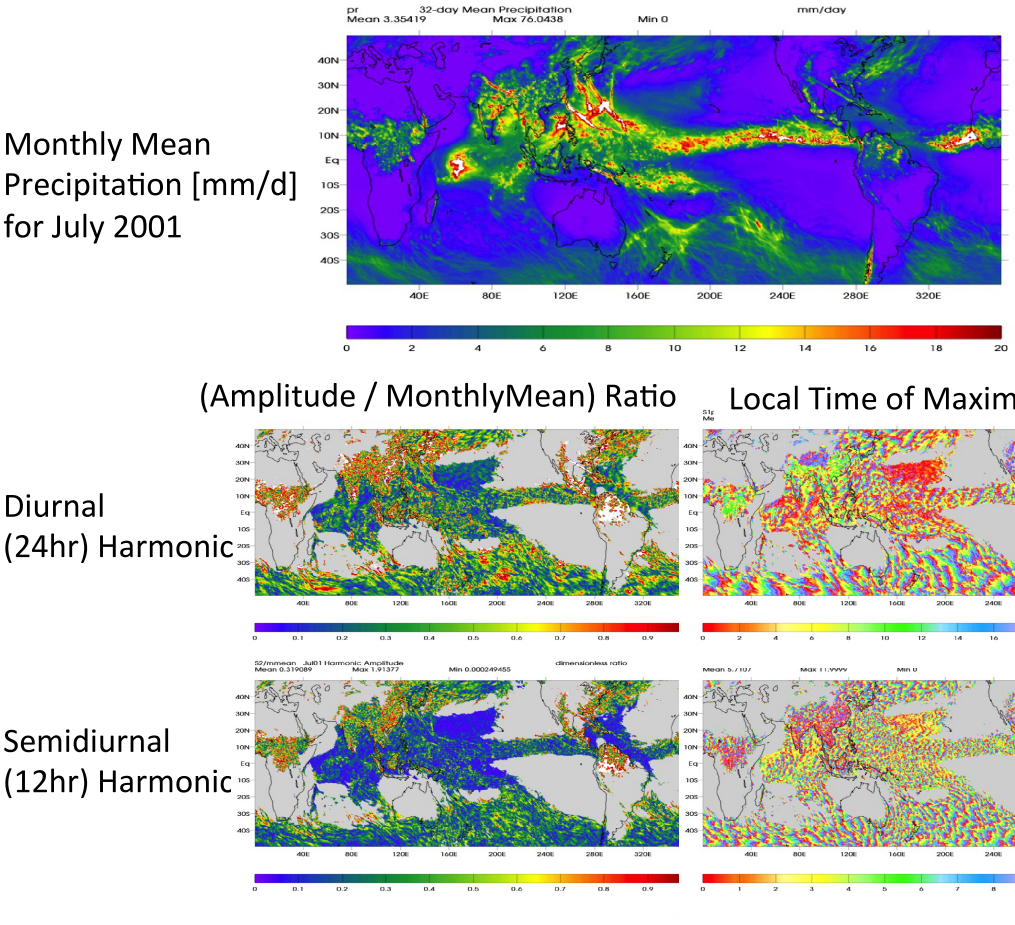

Appendix

In the tropical oceans, the 12-hour component of precipitation maximizes around 6 AM / PM and has roughly half the amplitude of the 24-hour component. The latter also maxizes in early morning, so combining the two harmonics gives a curve like this:

Out[6]=

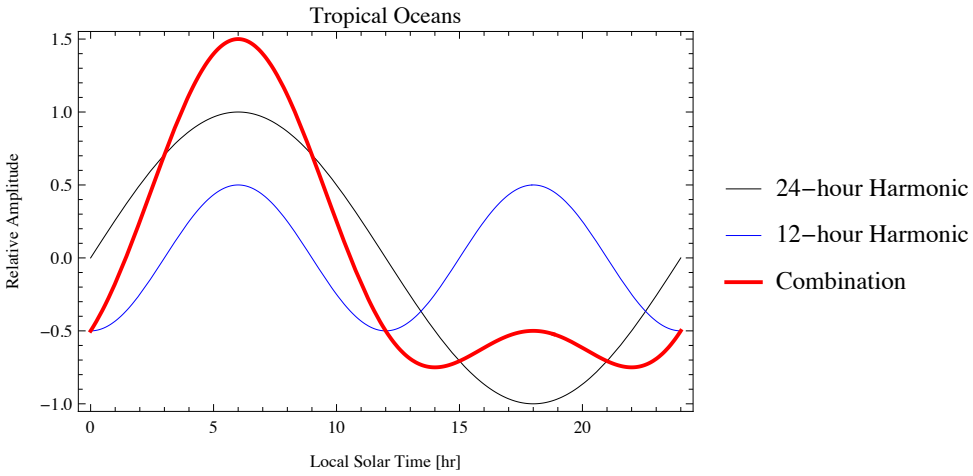

Over tropical land, 12-hour component of precipitation again maximizes around 6 AM / PM, but the 24-hour component now maximizes in late afternoon. The combination of the two again reinforces the 24-hour peak:

Out[7]=

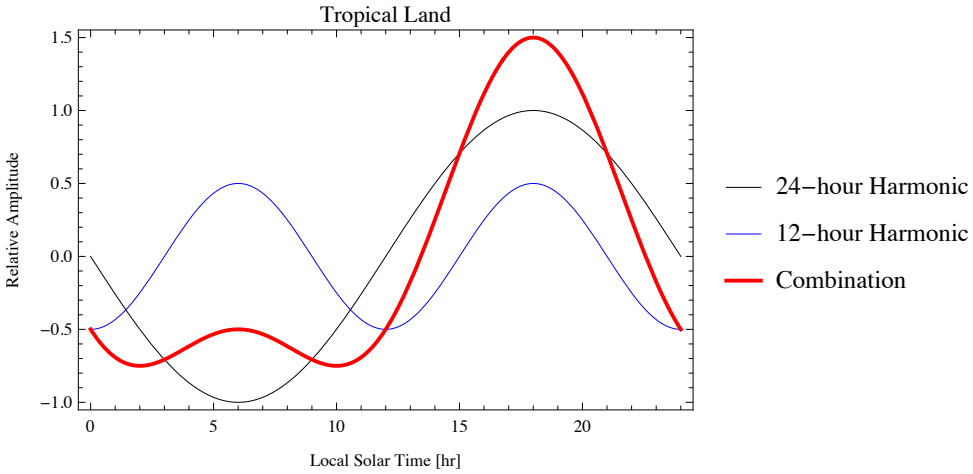

For some readers, the reinforcement of different harmonics at one time-point and their cancellation elsewhere may be familiar from the representation of the Dirac delta-function $\delta(t) \propto \int_{-\infty}^{\infty} e^{i\omega t}\, d\omega$ (e.g. Elmore and Heald 1969, Problem 12.2.3).

References

C. Covey, A. Dai, D. Marsh and R. S. Lindzen: “The Surface-Pressure Signature of Atmospheric Tides in Modern Climate Models,” *Journal of the Atmospheric Sciences 68,* 495-514, 2011

C. Covey, A. Dai, R. S. Lindzen and D. Marsh: “Atmospheric Tides in the Latest Generation of Climate Models,” *ibid. 71*, 1905-1913, 2014

A. Dai and J. Wang, “Diurnal and Semidiurnal Tides in Global Surface Pressure Fields,” *ibid. 56*, 3874-3891, 1999

A. Dai and K. E. Trenberth: “The Diurnal Cycle and its Depiction in the Community Climate System Model,” *Journal of Climate 17*, 930-950, 2004

A. Dai, X. Lin and K.-L. Hsu: “The Frequency, Intensity, and Diurnal Cycle of Precipitation in Surface and Satellite Observations over Low- and Mid-Latitudes,” *Climate Dynamics 29,* 727-744, 2007

W. C. Elmore and M. A. Heald: *Physics of Waves*, McGraw-Hill, 1969

W. L. Gates and coauthors: “An Overview of the Results of the Atmospheric Model Intercomparison Project (AMIP I),” *Bulletin of the American Meteorological Society 80*, 29-55, January 1999

X. Jiang, N.-C. Lau and S. A. Klein: “Role of Eastward Propagating Convection Systems in the Diurnal Cycle and Seasonal Mean of Summertime Rainfall Over the U.S. Great Plains,” *Geophysical Research Letters 33*, L19809, 2006

K. Kikuchi and B. Wang: “Diurnal Precipitation Regimes in the Global Tropics,” *Journal of Climate 21,* 2680-2696, 2008

J. E. Kutzbach: “Empirical Eigenvectors of Sea-Level Pressure, Surface Temperature and Precipitation Complexes over North America,” *Journal of Applied Meteorology 6,* 791-802, 1967; see also M. Hirose and J. E. Kutzbach: “An Alternate Method for Eigenvector Computations,” ibid. *8,* p. 701

E. N. Lorenz: *Empirical Orthogonal Functions and Statistical Weather Prediction,* Statistical Forecasting Project Scientific Report No. 1, MIT Department of Meteorology, 1956 (http://www.o3d.org/abracco/Atlantic/Lorenz1956.pdf)

W. H. Press, S. A. Teukolsky, W. T. Vetterling and B. P. Flannery: *Numerical Recipes: The Art of Scientific Computing,* 3rd Ed., Cambridge University Press, 2007

K. E. Taylor: “Summarizing Multiple Aspects of Model Performance in a Single Diagram,” *Journal of Geophysical Research 106*, 7183-7192, 2001

J. Teixeira, D. Waliser, R. Ferraro, P. Gleckler, T. Lee and G. Potter, “Satellite Observations for CMIP5: The Genesis of Obs4MIPs,” *Bulletin of the American Meteorological Society*, in press 2014 (early online release at http://journals.ametsoc.org/doi/abs/10.1175/BAMS-D-12-00204.1)

K. E. Trenberth, D. P. Stepaniak and L. Smith, “Interannual Variability of Patterns of Atmospheric Mass Distribution,” *Journal of Climate 18,* 2812-2825, 2005

D. N. Williams and the UV-CDAT Project Team: “Ultrascale Visualization of Climate Data,” *IEEE Computer*, September 2013, 68-75